17th World Conference on Earthquake Engineering, 17WCEE
Sendai, Japan - September 13th to 18th 2020

STRUCTURAL BEHAVIOR OF THE DRY PARTITION WALL WITH LIGHT-GAUGE STEEL

Y. Sato[(1)], F. Sakuraba[(2)], S. Motoyui[(3)]

[(1)] *Researcher, Takenaka Corporation, satou.yasuaki@takenaka.co.jp*
[(2)] *Manager & Senior research engineer, Shimizu Corporation, f.sakuraba@shimz.co.jp*
[(3)] *Professor, Tokyo Institute of Technology, motoyui.s.aa@m.titech.ac.jp*

Abstract

While the seismic performance of structural members is improving, non-structural structural damages are prominent in recent earthquake damage. In 2016 Kumamoto earthquake, there was a building where the partition walls were severely damaged. Immediately after the earthquake, the building was demolished because it was difficult to continue using it. This damage example indicates that the partition wall damage not only affects the continued usability immediately after the earthquake, but may also significantly affect the life of the building. The partition wall is usually a composite structure (Light-Gauge-Steel wall) composed of a thin steel plate open-section member (LGS), gypsum board, and screws. Light-Gauge-Steel members and gypsum board are made of materials specified by Japanese Industrial Standards (JIS). However, the material properties required to design the earthquake resistant LGS walls are not clearly described in JIS. In addition, the LGS wall is designed according to the type and arrangement of members specified in the standard specifications, but the engineering standards for seismic performance requirements are unclear. In-plane or out-of-plane behavior is focused when studying on the structural characteristics of LGS walls. Among the few previous studies conducted in Japan and overseas, most of them are mainly focused on the in-plane structural characteristics of the LGS walls. In addition, the stiffness evaluation based on static tests is performed, and differences exist in the obtained conclusions. Therefore, the theoretical evaluation method to include the out-of-plane rigidity of the LGS walls has not been clarified so far.

In this study, this study aims to develop a numerical analysis model that can evaluate the rigidity and strength against the out-of-plane deformation for rational seismic design of the LGS wall. At first, basic material properties were clarified by uniaxial loading test and four-point bending test of gypsum board under normal temperature and humidity. Second, a tensile test and a short column compression test of a stud, which is one of the Light-Gauge-Steel members, were conducted to clarify the basic material properties. The effect of the lip of the stud on local buckling strength and buckling mode was clarified through numerical analysis. In addition, an elemental experiment was conducted to confirm the shear behavior of the screw joint. Finally, a numerical analysis model considering the shear behavior of the screw joint was developed. Using this numerical analysis model and the basic material characteristics reported in Part 1, the stiffness and proof strength against the out-of-plane deformation of the LGS wall were evaluated. The proposed numerical analysis model was validated by comparing it with the out-of-plane stiffness of the LGS wall obtained in the previous studies.

Keywords: Partition wall; Light-Gauge-Steel; Gypsum board; Material property; Out-of-plane deformation

1. Introduction

While the seismic performance of structural members is improving, non-structural structural damages are prominent in recent earthquake damage. In 2016 Kumamoto earthquake, there was a building where the partition walls were severely damaged, as shown in Fig.1. After the earthquake, the building was demolished because it was difficult to continue using it. This damage example indicates that the partition wall damage not only affects the continued usability after the earthquake, but may also significantly affect the life of the building. The partition wall is usually a composite structure composed of thin steel plate open-section members (Light-Gauge-Steel) called a runner and a stud, gypsum boards, and screws, as shown in Fig.2. In Japan, this kind of partition is called as LGS wall. Light-Gauge-Steel members and gypsum board are made of materials specified by Japanese Industrial Standards (JIS). Because of its excellent workability, it is most often used as the inner wall regardless of the type of main structure. However, the material properties required to design the earthquake resistant LGS walls are not clearly described in JIS. In addition, the LGS wall is designed according to the type and arrangement of members specified in the standard specifications [1], but the engineering standards for seismic performance requirements are unclear.

In-plane or out-of-plane behavior is focused when studying on the structural characteristics of LGS walls. Among the few previous studies [3,4,5,6] conducted in Japan and overseas, most of them are mainly focused on the in-plane structural characteristics of the LGS walls. On the other hand, there are very few previous studies on the out-of-plane structural characteristics of the LGS walls Against this background, the Study Group on LGS Wall Structural Properties was launched in 2017 under the consortium for building research and development in Japan, and several experiments were conducted on the out-of-plane structural properties of LGS walls[7]. The following conclusions on the out-of–plane structural characteristics of LGS wall were shown from those experiments [7].

1) The bending stiffness of LGS wall is obtained as a composite beam of gypsum board and stud.
2) The bending stiffness of LGS wall depends on the gypsum board installation states.
3) Maximum strength of LGS wall is determined by local buckling of studs for all specimens.

On the other hand, the previous study [3] concludes that "the out-of-plane stiffness of the LGS wall is calculated by ignoring the gypsum board and considering only the bending stiffness of the stud", and this result is not consistent with the conclusion in the previous study [7]. Therefore, the theoretical evaluation method to include the out-of-plane rigidity of the LGS walls has not been clarified so far.

In this paper, the material properties used for LGS walls were clarified by elementary experiments, and this study aims to develop a numerical analysis model that can evaluate the rigidity and strength against the out-of-plane deformation for rational seismic design of the LGS wall.

Fig. 1 – Damage of LGS wall in Kumamoto earthquake 2016

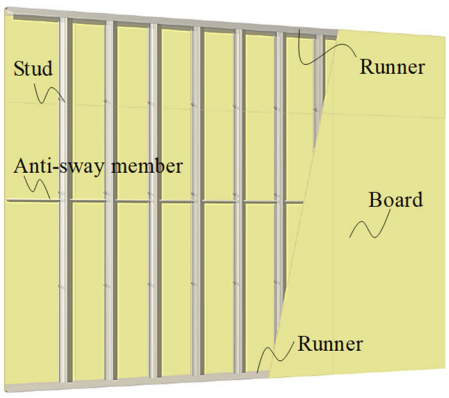

a) Overall view

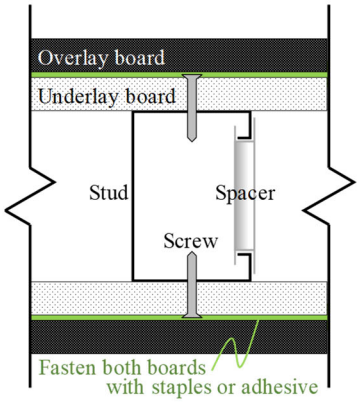

b) Sectional view

Fig. 2 – Structure of LGS wall

2. Mechanical properties of components of LGS wall

The studs, runners and gypsum board are each made of materials specified in Japanese Industrial Standards (JIS). The studs and runners are made of a hot-dip galvanized steel sheet defined by JISG3302, and only define a range in which the steel sheet has a yield point of at least 205 MPa and a tensile strength of at least 270 MPa. For this reason, the material properties of members that are actually widely used are ambiguous in structural design. For gypsum board specified in JISA6901, only the test method for gypsum board is specified, but there is not enough mechanical information to study the material properties of LGS walls.

In this section, first, the material properties of gypsum board are clarified by performing uniaxial loading test and 4-point bending test of gypsum board under normal temperature and humidity. Next, using a steel sheet sampled from the stud, the material properties of the hot-dip galvanized steel sheet are confirmed by a typical tensile test. Then, a short column compression test of the stud is performed to determine the determinant of the maximum strength of the stud. In addition, the mechanical properties of the system in which the stud and the gypsum board are joined by screws are discussed.

2.1 Gypsum board

Generally, the gypsum board is considered to have fibers of gypsum board in parallel along the flow of the production line. Therefore, as shown in Fig.3, the X direction parallel to the fibers of the gypsum board and the Y direction orthogonal to the fibers were defined. And, the test pieces for the uniaxial loading test were sampled with the laser cutter as shown in Fig.3. The compression test pieces were rectangular. On the other hand, the tensile test pieces were cut in half at the center section so as to break at the center of the test piece. Four types of gypsum boards were prepared: normal board thickness t = 12.5 mm, reinforced board t = 12.5 mm and 21 mm, and calcium silicate board t = 6 mm. These are the types widely used for LGS walls. In addition, these specimens were ordered from four gypsum board manufacturers. It is expected that there will be differences between manufacturers. The list of the compression test pieces is summarized in Table 1.

The tensile test pieces were cut out only in the X direction with a normal board thickness t = 12.5 mm of Manufacturer-A in order to focus on the stiffening effect of the surface paper of the gypsum board. Three test pieces were prepared. three test pieces were prepared. And, the tensile test pieces of the surface paper were also prepared. Four test pieces of the surface paper were obtained by removing only gypsum from two pieces of the gypsum board. As shown in Fig.4, The measurement are the load F_0 and the displacement u_0 measured by the measuring instruments mounted on the loading test machine, and the displacement $u_{1,2}$ of the gauge distance by two potentiometers. In the compression test pieces, the strain $\varepsilon_{1,2}$ were also measured by the strain gauges attached to the center of the surface papers. All test pieces were stored at the temperature of 20 ℃, and the humidity of 55% in the uniform indoor environment for at least one day. After that, these test pieces were set on the loading test machine and monotonically loaded in the compression and tension directions.

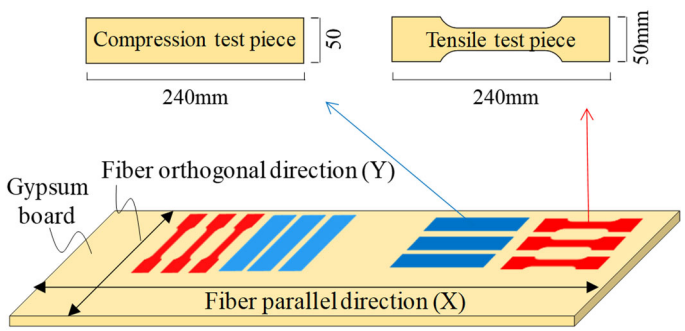

Fig. 3 – Concept of sampling test pieces

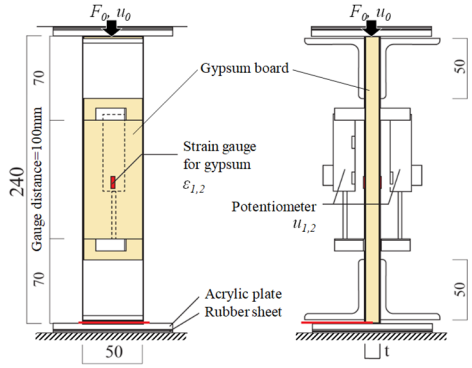

a) Front view b) Side view

Fig. 4 – Outline of uniaxial loading test

Fig.5 shows the stress-strain relationship of the compression test. Since it is difficult to put all the test results on the limited space of papers, Fig.5 shows an example of the normal gypsum board t = 12.5 mm of Manufacturer-A. The Young's modulus and maximum stress of all specimens obtained from the stress-strain relationship were recorded in Table 1. From Fig.6 and Table 1, there were three fracture types of the test pieces, but no difference in the maximum stress was observed among them. In order to confirm the material anisotropy at the Young's modulus and maximum stress of the gypsum board, Fig. 7 shows the correlation diagram of the material properties in the X direction and the Y direction (see Fig. 3) of the gypsum board. The Young's modulus and maximum stress tended to be lower in the Y direction than in the X direction. Further, the shape of the marker in Fig.7 indicates a difference between manufacturers, and a slight difference in material properties between the manufacturers can be confirmed.

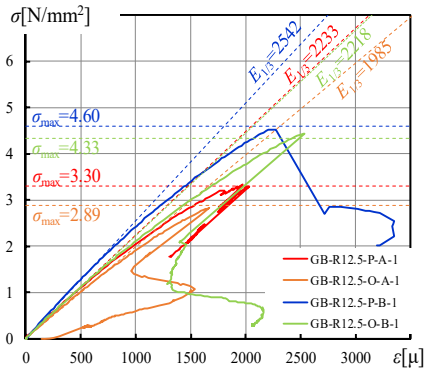

Fig. 5 – Stress-strain relationship in compression test

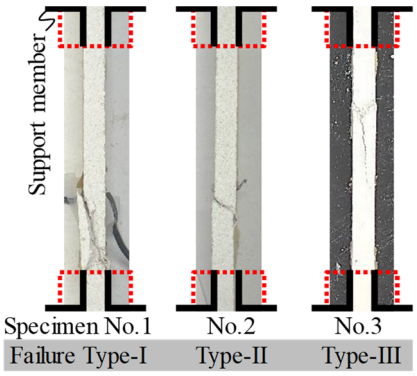

Fig. 6 –Failure type (e.g. GB-R12.5-P-A)

Table 1 – Test piece list

Specimen No.		Average width [mm]	Average Length [mm]	Average Thickness [mm]	Mass [g]	Density [g/cm³] Individua	Density [g/cm³] Average	1/3 secant elasticity [N/mm²] Individua	1/3 secant elasticity [N/mm²] Average	Maximum compressive stress [N/mm²] Individual	Maximum compressive stress [N/mm²] Average	Failure type
GB-R-12.5-P-A	1	50.45	240.50	12.69	102.00	0.66	0.68	2192	2233	3.33	3.30	I
	2	49.65	239.85	12.65	103.50	0.69		2258		3.21		II
	3	49.63	239.33	12.64	102.90	0.69		2251		3.36		III
GB-R-12.5-O-A	1	50.18	240.18	12.75	103.10	0.67	0.68	2048	1985	2.83	2.89	I
	2	49.25	239.45	12.79	102.60	0.68		1833		2.72		II
	3	49.43	239.60	12.78	103.90	0.69		2074		3.13		II
GB-R-12.5-P-B	1	49.43	239.60	12.72	103.10	0.68	0.68	2549	2542	4.53	4.60	II
	2	49.68	239.80	12.74	103.20	0.68		2538		4.55		I
	3	49.63	239.63	12.72	103.20	0.68		2541		4.72		I
GB-R-12.5-O-B	1	49.63	239.60	12.75	103.90	0.69	0.69	2117	2218	4.43	4.33	II
	2	49.65	239.70	12.68	106.10	0.70		2367		4.26		II
	3	49.60	240.10	12.78	104.90	0.69		2171		4.30		I
GB-F12.5-P-A	1	50.10	240.10	12.74	118.00	0.77	0.77	3177	3090	5.01	4.88	I
	2	49.98	240.08	12.77	118.00	0.77		3083		4.63		II
	3	49.68	240.10	12.80	118.60	0.78		3010		4.99		III
GB-F12.5-O-A	1	50.13	240.10	12.74	119.50	0.78	0.78	2752	2749	4.53	4.36	I
	2	50.05	239.93	12.75	118.80	0.78		2686		3.93		II
	3	49.98	240.10	12.85	120.70	0.78		2809		4.63		I
GB-F12.5-P-B	1	50.20	239.53	12.72	117.60	0.77	0.77	2928	3073	6.09	6.05	I
	2	50.18	239.58	12.68	117.90	0.77		3086		5.74		II
	3	50.13	239.40	12.73	118.90	0.78		3206		6.32		I
GB-F12.5-O-B	1	49.83	239.90	12.74	120.90	0.79	0.78	2700	2700	5.91	5.47	II
	2	49.85	239.73	12.68	117.50	0.78		2746		5.47		II
	3	49.80	239.68	12.70	119.00	0.79		2655		5.03		I
GB-F21-P-A	1	50.30	240.33	21.31	197.50	0.77	0.77	2432	2654	5.47	5.24	I
	2	50.13	239.90	21.30	195.90	0.76		2710		4.97		I
	3	50.30	240.45	21.24	197.00	0.77		2821		5.28		I
GB-F21-O-A	1	50.13	240.70	21.30	196.60	0.77	0.77	2481	2484	4.74	4.52	II
	2	50.10	239.98	21.30	197.30	0.77		2488		4.44		I
	3	50.28	239.78	21.31	197.00	0.77		2484		4.38		I
GB-F21-P-B	1	49.78	239.80	21.17	197.20	0.78	0.78	3032	3041	5.91	5.73	I
	2	49.60	239.65	21.18	195.40	0.78		3018		5.61		II
	3	49.85	239.65	21.19	197.00	0.78		3073		5.67		I
GB-F21-O-B	1	49.75	239.83	21.18	196.70	0.78	0.78	2476	2583	4.24	4.54	I
	2	49.78	239.95	21.16	196.20	0.78		2626		4.75		II
	3	49.45	239.40	21.18	195.30	0.78		2648		4.65		I
Ca-P-C	1	50.65	237.70	17.94	177.10	0.82	0.82	3812	4303	8.71	10.59	II
	2	49.91	237.88	18.25	175.80	0.81		4270		11.04		II
	3	49.59	237.33	17.85	173.50	0.83		4828		12.03		II
Ca-O-C	1	49.10	238.48	18.11	172.00	0.81	0.81	3682	3627	9.07	9.82	II
	2	49.63	238.50	18.23	174.60	0.81		3635		9.94		III
	3	49.76	239.23	18.08	173.70	0.81		3564		10.44		II
Ca-P-D	1	50.28	240.40	18.21	185.20	0.84	0.84	5031	5065	13.74	14.15	III
	2	50.35	240.10	18.14	185.80	0.85		5204		14.85		I
	3	50.30	240.10	18.30	183.70	0.83		4960		13.85		I
Ca-O-D	1	50.30	240.40	18.02	187.60	0.86	0.86	4535	4576	13.31	13.31	III
	2	50.30	240.08	18.20	188.40	0.86		4588		13.56		I
	3	50.30	240.03	18.03	187.30	0.86		4606		13.05		III

GB-R-12.5-P-A
a) b) c) d) e)

Ca-P-C
a) d) e)

a) Material GB : Gypsum board, Ca : Calcium silicate plate
b) Board Type R : Normal, F : Reinforced
c) Thickness 12.5mm, 21mm
d) Direction P : Parallel to fiber, O : Orthogonal to fiber
e) Manufacturer A, B, C, D

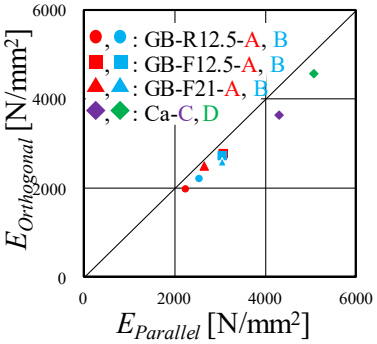

a) Young's modulus *E*

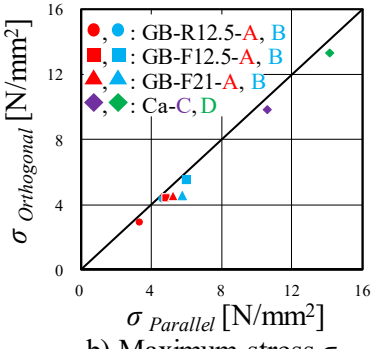

b) Maximum stress *σ*

Fig. 7 – Gypsum board material anisotropy

The results of the tensile test shown in Fig.9 are shown by the relationship between the load per unit width (F_0/B) obtained by dividing the load by the width B of the test piece and the strain between the gauge points. In Fig.9, the gypsum board was separated into the surface paper and the gypsum using Eq. (1) obtained by considering the distribution of strain and stress in the cross section of the gypsum board as shown in Fig.8. Since the process of removing the gypsum is a cause of uncertainty in the thickness of the surface paper, the rigidity of each materials are investigated by Et, which is the Young's modulus multiplied by the thickness of each materials.

$$F_0/B = E_0 t_0 \varepsilon_t = \left(2E_{Pa}t_{Pa} + E_{Gy}t_{Gy}\right)\varepsilon_t \quad (1)$$

Where F_0; applied load, B; width of gypsum board, E_0, t_0; Young's modulus and thickness of the composite material of surface paper and gypsum, ε_t; axial tensile strain of cross section, E_{Pa}, t_{Pa}; Young's modulus and thickness of the surface paper, E_{Gy}, t_{Gy}; Young's modulus and thickness of the gypsum. E_0t_0 and $E_{Pa}t_{Pa}$ were obtained from Fig.9 and the curve of gypsum was obtained from the difference of the composite to the face paper. From this figure, it is considered that the gypsum crack was gradually generated at a strain of about 500 μ. Finally, the surface papers broke at the point of maximum stress. It is considered that the increase in the stress after the gypsum cracking is due to the effect of tension stiffening between the gypsum and the surface papers. The material properties of the surface paper and the gypsum obtained in Fig.9 are used for the numerical analysis model of the LGS wall described later.

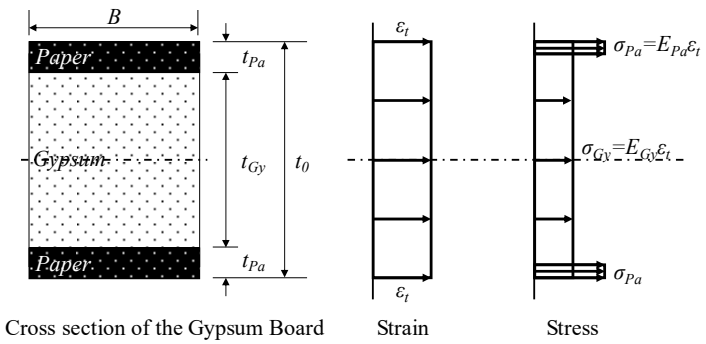

Fig. 8 – Concept of strain and stress distribution

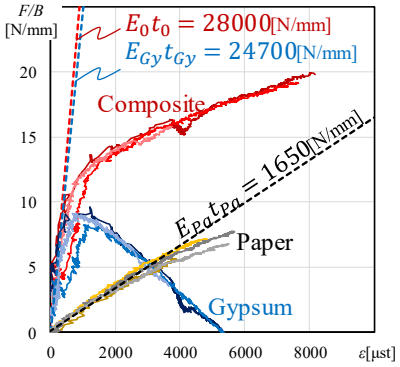

Fig. 9 – F_0/B-strain relationship in tensile test

Next, the bending test was conducted to determine the bending stiffness of the LGS gypsum board subjected to out-of-plane forces. In order to reduce the influence of the shear deformation of the specimen, a four-point bending test in which the specimen had a pure bending section was adopted. Fig.10 shows the outline of the bending test. Similarly the tensile test piece, the bending test pieces were cut out only in the X direction of the manufacturer A having the normal board thickness t=12.5 mm. The measurement items are load F_0, displacement u_0, and displacement by the potentiometer shown in Fig.10 as in the uniaxial loading test. In order to obtain the rotation angles θ at the end of the pure bending section, a rigid iron plate fixed to the test piece with an adhesive was used as the target of the potentiometer.

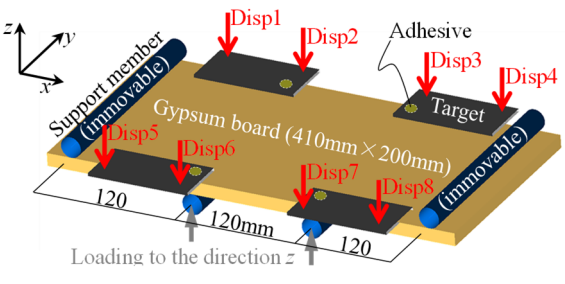

Fig.10 – Concept of 4-point bending test

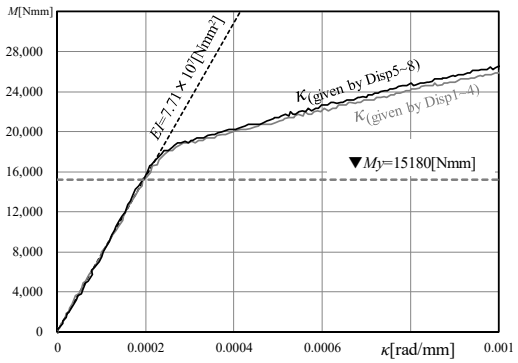

Fig. 11 – Relationship between M and κ

Fig. 11 shows a bending moment curvature diagram of the test piece. It is unlikely that thin surface paper can directly bear the bending moment. However, it was clear in the tensile test that the surface paper worked effectively against the axial tensile force. On the other hand, gypsum works effectively against axial compression force. Therefore, the gypsum board subjected to the bending moment is similar in concept to the section stress of the reinforced concrete beam. Applying this concept, the strain and the stress distribution of the gypsum board cross section when the gypsum board is elastic is shown in Fig. 12, and the stress state in the yield state is considered as shown in the right of Fig. 12. As described above, when it is considered that the surface paper on the compression side of the gypsum board cross section is not related to the compression force, the out-of-plane bending rigidity when the gypsum board is elastic can be written as follows.

$$\frac{M}{\kappa} = \left[E_{Pa}t_{Pa}(t_0 - y)^2 + \frac{1}{3}E_{Gy}(t_0 - y)^3 + \frac{1}{3}E_{Gy}y^3\right]B \tag{2}$$

Here, the surface paper is considered to be negligibly thin ($t_{pa} \fallingdotseq 0$). And the neutral axis ratio; $\acute{y} = \frac{y}{d} = \frac{2dnp_t + {t_0}^2}{2d(np_t + t_0)}$, the Young's modulus ratio of the gypsum and the surface paper; $n = \frac{E_{Pa}}{E_{Gy}}$, the tensile paper ratio; $p_t = \frac{t_{Pa}}{d}$, . On the other hand, the ultimate bending moment can be written as:

$$M = E_{Pa}t_{Pa}\varepsilon_{ty}Bj \tag{3}$$

Here, $e = t_0 - E_{Pa}t_{Pa}\varepsilon_{ty}/{}_{max}\sigma_c$, the yield strain of surface paper; ε_{ty}, the maximum compressive stress of the gypsum (reference to Table 1); ${}_{max}\sigma_c$, the distance between the tensile force of the surface paper and the compressive force of the gypsum; $j = (t_0 + e)/2$, and the stress of the gypsum is simply assumed to be the rectangular block. The black dashed line in Fig. 11 is the bending stiffness calculated by Eq. (2), and the gray dashed line is the ultimate moment calculated by Eq. (3). Both are close to the test results.

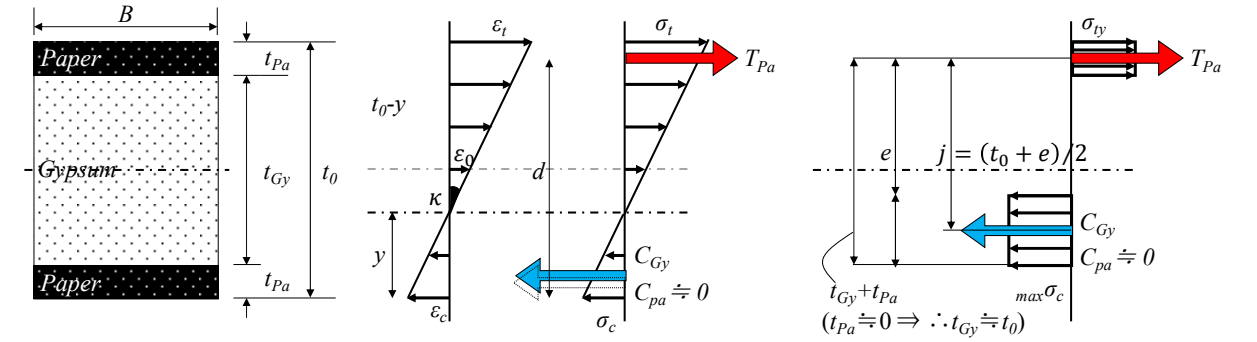

Cross section of the Gypsum Board | Strain | Stress (Elastic state) | Stress (the surface paper and the gypsum are yield)

Fig. 12 – Analysis for the bending test

2.2 Light-Gauge-Steel members (LGS)

The tensile test was performed to obtain the material properties of the stud. The test pieces were prepared in accordance with the provisions of the test piece No. 13B with reference to JISZ2241 as shown in Fig.13. The studs were picked up one by one from two production lots in order to take into account variations in material properties. Then, three test pieces were taken out from the web and flange of each studs. Fig.14 shows the stress-strain relationship of each test pieces obtained in the tensile test. Table 2 shows the yield point, tensile strength, elongation at break, and yield ratio obtained by averaging the results of the three test pieces. From these results, it was found that the yield point and the tensile strength of the stud were about 1.5 times the JIS reference values (yield point ≧ 205 MPa, tensile strength ≧ 270 MPa). The variation of the yield point by the production lot was about 20%. Since the yielding was clearly shown, the influence of the plastic working of the flange is considered to be small.

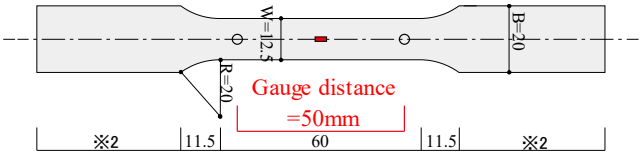

Fig. 13 – The Shape of the test piece

Table. 2 – The material property of specimen

Specimen name		Yeild strength σ_y[N/mm^2]	Ultimate strength σ_u[N/mm^2]	Fracture strain [%]	Yeild ratio [%]
Lot-1	Flange	330	404	31.7	81.9
	Web	311	396	32.6	78.6
Lot-2	Flange	340	406	26.6	83.8
	Web	355	402	30.3	88.2

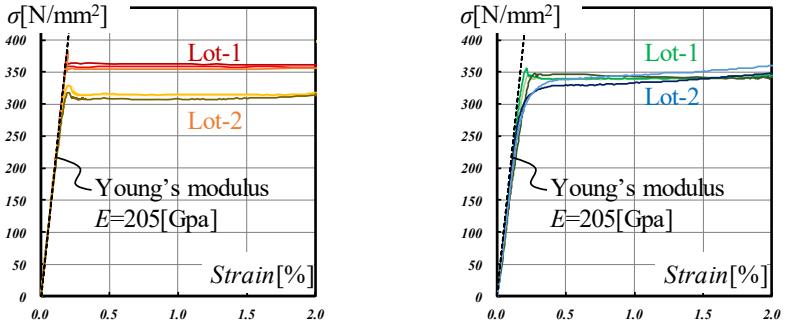

a) The web of stud b) The flange of stud

Fig. 14 – The stress-strain relationship of each test pieces

Next, considering that the stud of the LGS wall is mainly the member to be bent, the buckling strength when the axial force (N) and the bending (M) are simultaneously received is evaluated using the analysis model of Fig.15. The stud was created with shell elements. The boundary condition at the end of the stud was simply supported. With reference to the tensile test results in Fig.14, the material properties of the steel were the bilinear type. Before applying force, an initial imperfection was introduced with reference to the eigenmode obtained by eigenvalue analysis so that the maximum displacement was 1/50 of the thickness of the stud. In this analysis, a forced displacement in which the expansion (δ) and the rotation (θ) shown in Fig.15 were set to a constant ratio $\phi = \delta / \theta \in [\infty, -h/2, -h/6, 0, h/10]$ was applied to the side of the stud.

First, the validity of the analytical model was examined by comparing it with a short column compression test of a purely compressed ($\phi = \infty$) stud. In the test, three specimens shown in Fig.16 were prepared, and the upper and lower ends of the specimen were carefully cut so that a uniform compressive force was applied to the specimen, and a flat plate was installed. The load P and the displacement δ were measured by a load cell and a displacement meter mounted on the compression tester. The surface strain at the center of the specimen was measured with strain gauges. Fig.17 shows the load-displacement relationship, and the analysis result is the black dotted line. Due to the extremely large width-to-thickness ratio between the stud web and the flange, the local buckling occurred in the elastic region. The load-displacement curve (Fig. 17) obtained by the numerical analysis and the test are almost the same. These results confirmed the validity of the numerical analysis.

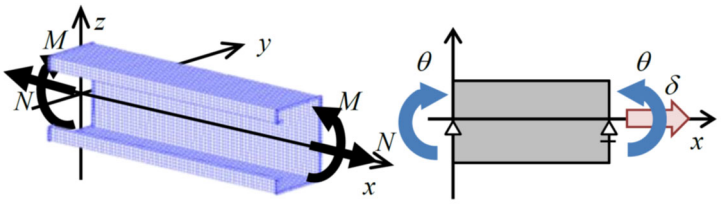

Fig. 15 – Concept of Analysis model of the stud

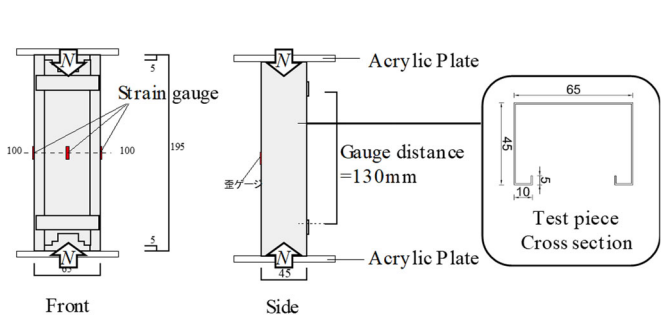

Fig. 16 – Concept of the purly compressive test

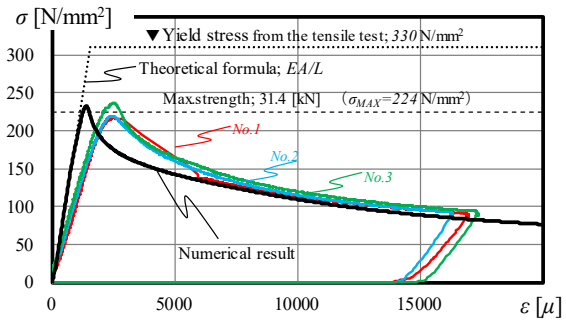

Fig. 17 – The stress-strain curve of the stud

Next, Fig.18 shows a bending-curvature relationship. Fig.19 redraws the result of Fig.18 by the value obtained by dividing the apparent axial force of the compression flange defined by the following equation by the yield axial force of the flange ($N_{FY}=A_F\times\sigma_Y$). The horizontal axis of Fig.19 is a value obtained by dividing the average contraction by the elastic yield contraction.

$$N_F = \left(\frac{N}{A} - \frac{M}{Z}\right) A_F \tag{4}$$

Where Z is the section modulus for the entire section of the stud and A_F is the flange cross-sectional area of the stud. Eq. (4) holds only for elasticity, however N_F is used for Eq. (4) because the target plate buckling is the elastic buckling. It can be understood from Fig.18 that the relationship between the compressive force of the flange and the average shrinkage can be evaluated almost uniformly by organizing in this way. Fig.20 shows the transition of each case in the *NM* space. Except in the case of pure compression in which the effect of axial force is large, it is confirmed that the buckling decreases the strength immediately after reaching the initial buckling strength line indicated by the dashed-dotted blue line. In addition, as for the result of pure compression ($\phi=\infty$), the proof stress decreased before the blue dashed line. This is because the web buckling precedes. Even if only lateral force is applied to the studs of the LGS wall targeted here, not only bending but also axial force as a composite beam effect is generated, but the axial force ratio does not become extremely large, so the blue solid line It can be said that the local buckling strength can be generally evaluated.

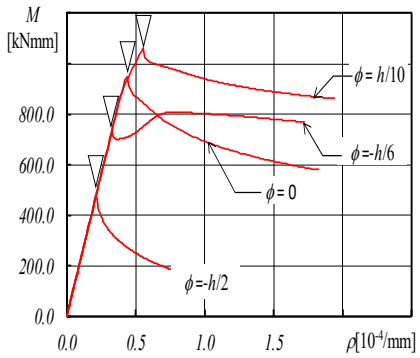

Fig. 18 – Relationship between bending moment and curvature

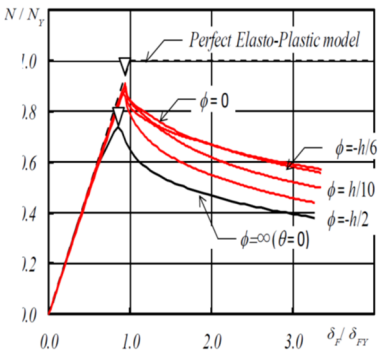

Fig. 19 – Relationship between axial force and elongation

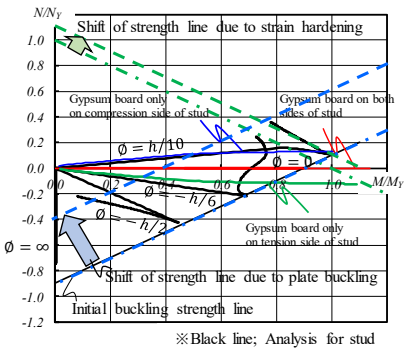

Fig. 20 – Interaction of axial force and bending moment

2.3 Connection LGS with gypsum board using Screws

The screw joint is composed of elements as shown in Fig.21. By replacing this with the numerical analysis model shown in Fig.21, the theoretical formula for evaluating the displacement behavior of the

screw joint is proposed. The bearing force of the gypsum board received by the screw is evaluated by a spring arranged on one side. The relationship between the shear force P_A (maximum proof stress P_{AU}) acting on the screw tip (point A) and the displacement u_A of the screw at point A (Fig. 21) is expressed by the following formula using the board thickness h.

$$P_A = K_S u_A + \mu N, \quad K_S = \frac{1+\alpha}{4+\alpha}\bar{k}h, \quad \alpha = \frac{K_A}{\bar{k}h^3/12} \tag{5}$$

$$P_{AU} = \left[\sqrt{2+\beta} - 1\right]F_b h + \mu N, \quad \beta = \frac{M_{AP}}{M_{bP}}, \quad M_{bP} = \frac{F_b h^2}{4}, \tag{6}$$

Here, $\bar{k}$ and F_b are the bearing stiffness and strength per unit area, μ and N are the friction coefficient and the contact force between the gypsum board and the stud, and K_A and M_{AP} are the rotational spring stiffness and the strength of the screw stud joint. Four tests were conducted to determine the physical properties of the screw joint required for this equation. Unless otherwise specified, the test was conducted on three boards each of 9.5 mm and 12.5 mm thick boards and 12.5 mm and 21.0 mm thick reinforced boards in order to take into account the variation of test pieces. Each material properties of the screw joint were obtained as follows from the four tests; $\bar{k}$ = 80 [N / mm] and F_b=32 (Reinforced), 26 (Normal) [N / mm], K_A =16900[Nmm / rad] and M_{ap}=1650 [Nmm]. And it was found that the coefficient of friction was independent of W, and μ=0.35 for all boards, regardless of the type and thickness of the board.

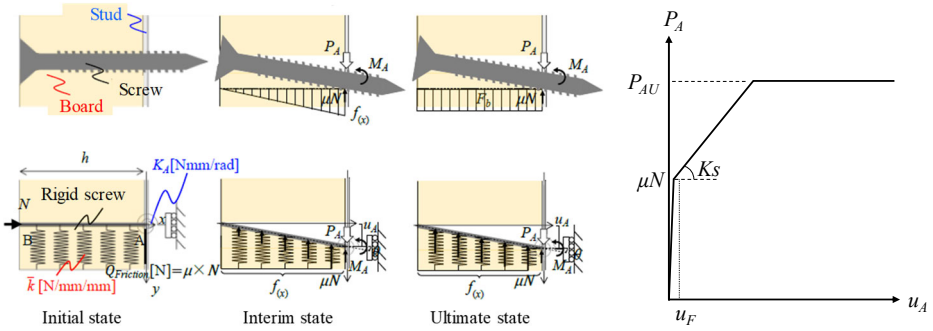

Fig. 21 – Mechanical model of the screw joint

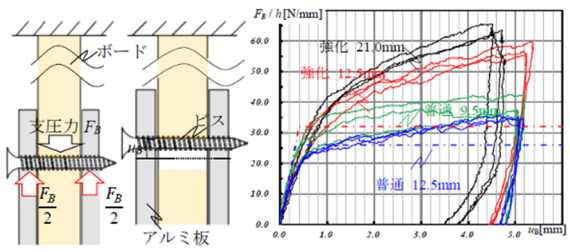

Fig. 22 – Bearing test of the screw joint

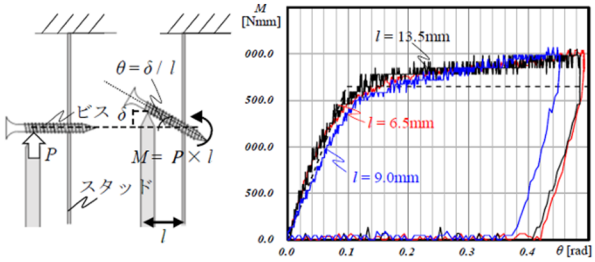

Fig. 23 – Rotation test of screw and stud joint

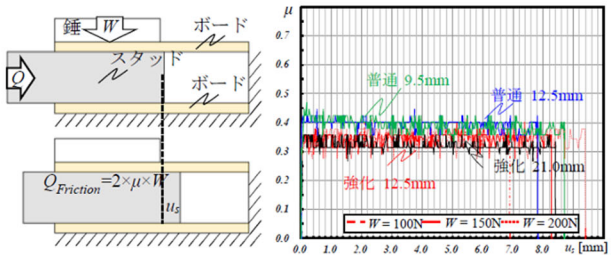

Fig. 24 – Stud and gypsum board friction test

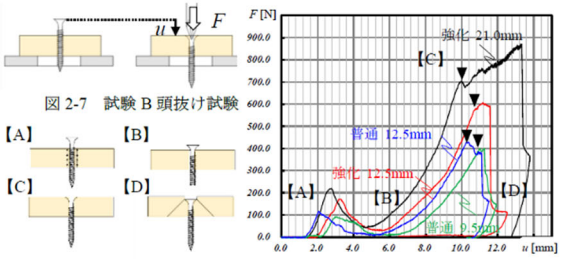

Fig. 25 – Screw head push test

In order to examine the validity of Eq. (5) and Eq. (6) using the physical property values obtained in the tests of Fig. 20 ~ Fig. 24, the shear test of the screw joint in as shown Fig. 26 was performed. The load P_A and the relative displacement u_A between the board and the stud were measured.

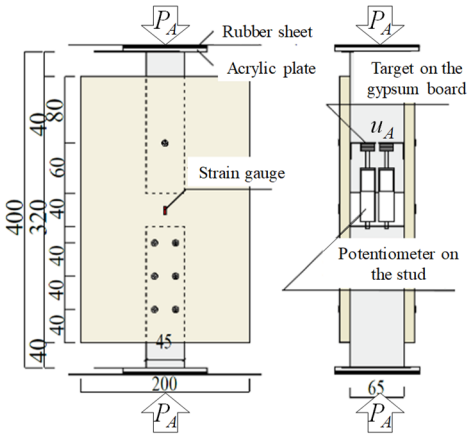

Fig. 26 – Concept of the Shear test of screw joint

The test was performed on four types of gypsum boards. Here, the load-displacement relationship of the test results is shown in Fig. 27 using two types of boards as examples. When the shear stiffness and the maximum strength obtained from Eq. (5) and Eq. (6) are plotted with blue lines in the test results, the shear behavior of the screw joint can be generally evaluated in a trilinear type. The initial stiffness was found to be due to frictional forces. However, the point at which the initial displacement occurs varies depending on the test pieces. Therefore, Eq. (5) and Eq. (6) with the point at which the displacement occurs as the lower limit are shown by the red lines in Fig. 27. In addition, comparing the results of the cyclic loading test in Fig. 28 with the results of the monotonic loading test in Fig. 27, it can be seen from the initial stage that the repeated loading has a displacement at the lower limit of the monotonic test result. In order to take into account the variation of the test pieces, the lower limit value (red line) in Fig. 27 and Fig. 28 is used as the material property of the screw joint used in the numerical analysis.

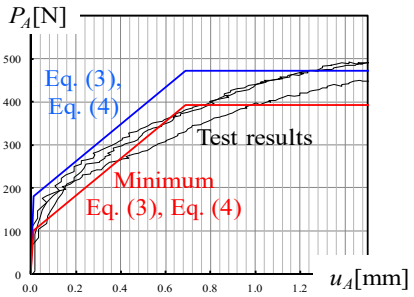

a) Normal board 12.5mm

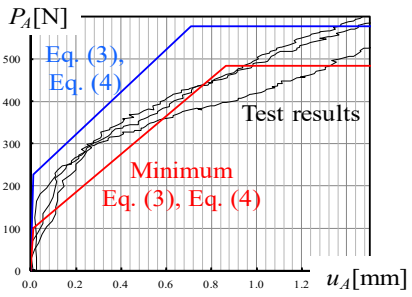

b) Reinforced board 21mm

Fig. 27 – The monotonic loading test

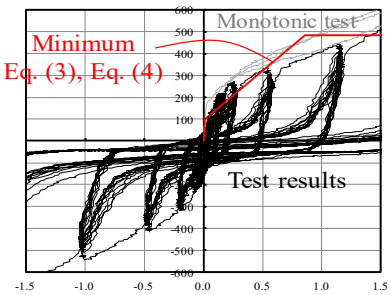

Reinforced board 21mm

Fig. 28 – The cyclic loading test

3. Evaluation of the out-of-plane deformation of the LGS wall

Numerical analysis including the inelastic region is performed by reflecting the mechanical characteristics of the stud, gypsum board and screw joint obtained so far. By comparing the results with the previous experiments [7], the mechanical properties of each member that have been clarified so far and the validity of the numerical analysis model produced by assembling them are examined. From the previous experiments [7], the specimens where the gypsum board is most likely to affect the rigidity and proof stress of the LGS wall (image of the specimen cross section in Fig.

30a) and the specimens that are less likely to affect (the image of the specimen cross section in Fig. 30b) are compared. Specimens with gypsum boards on both sides of the studs are assumed to perform the average behavior of the two types of specimens described above.

Fig. 29 shows the concept of the analysis model. Beam elements were all applied to the surface paper, gypsum, and studs of the gypsum board. The surface paper of the gypsum board and the gypsum are connected by the rigid body, and the stud and the gypsum are joined by a screw joint having material properties of a trilinear type shown in Fig. 27 Since the gypsum board had a reinforced board t = 21 mm, the F_0/B-strain relationship in tensile test in Fig. 9 of the reinforced board was obtained by the tensile test (Fig. 30). The material properties of the studs were the bilinear with reference to the results shown in Fig.14.

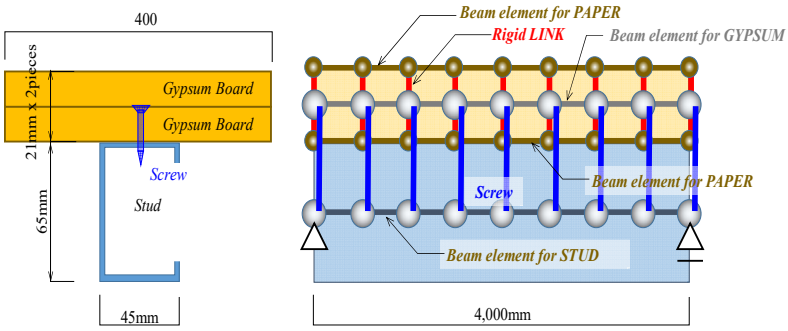

Fig. 29 – Concept of the numerical analysis model for LGS wall

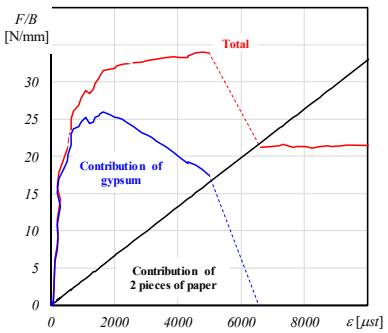

Fig. 30 – F_0/B-strain relationship in tensile test

The analysis results are compared with the experimental results [7] through the relationship between the center load F and the center displacement Uc in Fig. 29. In Fig. 31, the analysis results are located in the middle between the stiffness of the perfect composite of the gypsum boards and the studs and the stiffness of without the gypsum boards, confirming the imperfect combination effect of the stud and the board. The out-of-plane performance was evaluated accurately with any of the analysis results, and the validity of the numerical analysis model was confirmed. When this analysis result is compared with the N / N_Y-M / M_Y relationship in Fig. 20, buckling occurs at $1.0M_Y$ in the test specimen with the gypsum board on the compression side of LGS wall (Fig. 30b). On the other hand, the results of the test piece with the gypsum board on the tensile side of LGS wall (Fig. 30a) showed that the buckling at $0.8M_Y$ caused the stud strength to change by about 20%.

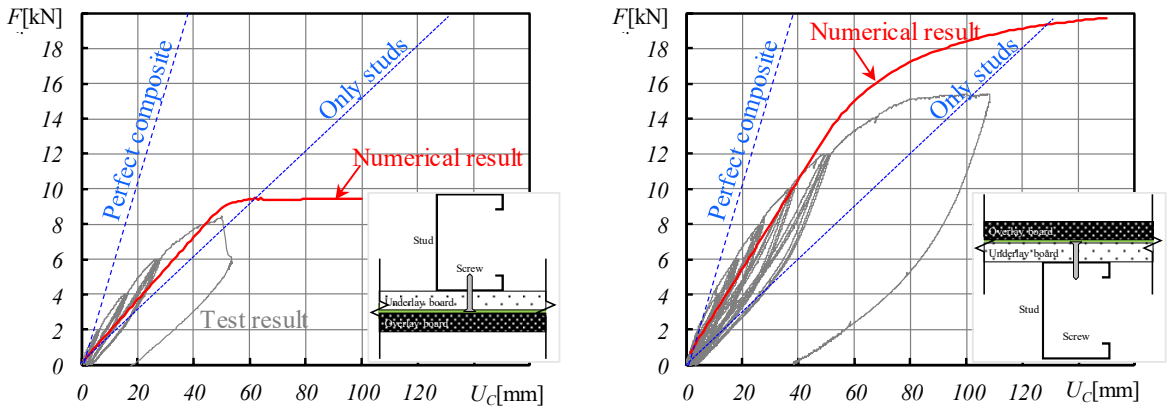

Fig. 30 – The force - displacement curve on the center of LGS wall

4. Conclusion

In this paper, the basic mechanical properties were clarified by conducting element tests on the studs, boards and screw joints which are the components of LGS wall. Then, the numerical analysis model of LGS wall considering these mechanical properties were constructed, and the rigidity and the strength were studied by comparing with the experimental results. The details of the conclusion are shown below;

1) The characteristics of the gypsum board with respect to the out-of-plane bending moment can be explained using the Young's modulus and the maximum stress obtained in the uniaxial loading test of the gypsum board.

2) The theory of the reinforced concrete can be applied to gypsum board subjected to out-of-plane bending moment. However, the face paper of the gypsum board does not resist the compressive force.

3) In the material properties of the stud, the yield point and the tensile strength were about 1.5 times the JIS reference values (yield point $\geqq$ 205 MPa, tensile strength $\geqq$ 270 MPa).

   The shear characteristic of the screw joint is generally considered as a trilinear type using the physical properties ($\bar{k}$, F_b, K_A, M_{ap}, μ).

4) The numerical analysis model considering the above contents showed that the rigidity and the strength of the LGS wall against the out-of-plane can be evaluated by comparison with the previous experimental results.

5. Acknowledgements

This work was supported by JST Program on Open Innovation Platform with Enterprises(JPMJOP1723), "Study on seismic damage control of lightweight steel-substrate dry-type partition walls" in the Consortium for Building Research and Development. And we gratefully acknowledge the work of Mitsuaki Ogawa who is a graduate student of Tokyo Institute of Technology.

6. References

[1] Ministry of Land, Infrastructure, Transport and Tourism (2013): Japanese Standard Specification for Public Building Construction.

[2] M Kato, T Matsumiya, K Suita, Y Matsuoka, M Nakajima (2007): Seismic performance and damage evaluation of drywall partition. Journal of structural and construction engineering (Transactions of AIJ), No.614, 139-146.

[3] R Minatogawa, S Motoyui, Y Sato, Y Sasaki (2013): Study on Anti-Plane Structural Property of Walls with Light-Gauge Steel. *Summaries of Technical papers of annual meeting Architectural Institute of Japan*, 1053-1054.

[4] K Ogihara, T Seike, M Osako, F Hayakawa, H Taga (2018): Development of Reduction Method for Seismic Damage to LGS Partition Wall (Part 2. Static loading test of LGS partition walls with various height). *Summaries of Technical papers of annual meeting Architectural Institute of Japan*, 1075-1076.

[5] Luigi F, Tatiana P, Raffaele L (2018): Out-of-plane seismic design by testing of non-structural lightweight steel drywall partition walls. *Thin-walled Structures*, Vol.130, 213-230.

[6] E Tanaka, T Terada, F Sakuraba, H Uchimoto, Y Ogawa, F Murota (2012): Anti-plane static loading tests on partition walls with light-gauge steel. *AIJ Journal of Technology and Design*, Vol.18, No.39, 575-578.

[7] T Someno, K Harayama, W Nitta, Y Sato, S Inai, et.al (2018): Development of Reduction Method for Seismic Damage to LGS Partition Wall (Part 3. Out of Plane Static Loading Tests on Vertical Installed LGS Partition Walls). *Summaries of Technical papers of annual meeting Architectural Institute of Japan*, 1077-1078.

